

FLIGHT STABILITY OF A FLYING WING MADE FROM SOLID FOAM

Maksym PETRENKO^{1*}, Peter GAŠPAROVIC¹

¹Technical University of Kosice Faculty of Aeronautics, Rampova 1731/7, 040 01 Kosice, Slovakia

*Corresponding author. E-mail: max.petrenko7@gmail.com

Abstract. This paper presents an investigation into the static and dynamic flight stability of a tailless flying wing made from solid foam (EPP). In the absence of traditional tail surfaces, the aerodynamic design uses a reflexed airfoil along with a carefully positioned center of gravity for maintaining longitudinal stability. The research integrates numerical simulations, wind tunnel tests, and actual flight trials to assess the model's performance under various flight conditions. Although the foam structure allows for cost-effective prototyping, it introduces a level of structural flexibility that can impact measurement accuracy and stability. The findings show that a well-constructed flying wing provides sufficient stability; however, materials such as EEP are too flexible for static testing in the wind tunnel, although they are good in dynamic flight.

Keywords: stability, flying wing, wind tunnel, tailless aircraft.

1. INTRODUCTION

Flight stability is a fundamental aspect of aircraft design, directly influencing controllability, performance, and safety. Conventional aircraft typically use horizontal and vertical stabilizers for stability, making their analysis relatively simple and well-established. In contrast, tailless designs, such as flying wings, present challenges. The lack of traditional tail surfaces restricts pitch and yaw stability, which invalidates many classic stability assumptions [1].

Flying wings remove the traditional tail, integrating all aerodynamic surfaces into a blended wing-body design. This approach provides multiple benefits—including reduced drag, enhanced lift-to-drag ratio, and potential stealth capabilities—but also introduces good aerodynamic and control challenges **Chyba! Nenašiel sa žiaden zdroj odkazov..** The primary issue is the lack of tail surface, which compromises longitudinal and directional stability. When these surfaces disappear, conventional simplifications lose validity, resulting in unreliable aircraft behavior **Chyba! Nenašiel sa žiaden zdroj odkazov..**

This study focuses on evaluating the static and dynamic stability of a flying wing constructed from solid foam. Using XFLR5 simulations, wind tunnel testing, and live flight trials with instrumented prototypes, we analyze aerodynamic behavior and assess the impact of low-cost, flexible construction. Our goal is to establish a practical methodology for analyzing tailless aircraft and support their application in UAVs and innovative manned platforms.

2. STABILITY OF TAILLESS AIRCRAFT

We can define the stability of flight in two main types: static and dynamic. Static stability ensures that after a small disturbance, restoring aerodynamic forces act in the correct direction. Dynamic stability, on the other hand, describes the aircraft's ability to return to equilibrium over time without external input.

We employ a body-fixed XYZ coordinate system. In trimmed flight, the net moments around the center of gravity must equal zero [6]. These moments follow the right-hand rule: when your thumb is aligned with an axis, the curl of your fingers indicates the positive rotational direction around that axis [6].

2.1. Longitudinal stability

Longitudinal stability allows an aircraft to retain or regain a stable flight path without elevator input. The aircraft is modeled as a flat object, under the assumption that the center of mass is not greatly displaced vertically [2].

Static longitudinal stability occurs only when the center of gravity (CG) to the aerodynamic center (AC) is located in front of the aerodynamic center (AC) [1]. The larger the distance between these two points, the more pronounced is the resulting stability. This is named as the static margin (SM), usually stated in ratio to the mean aerodynamic chord (MAC) [1].

The shape of the airfoil is fundamental for flying wing stability [4]. Traditional aircraft use cambered airfoils that need a tail surface, which leads to a negative pitching moment. To achieve balance, the CG is positioned behind the AC, see Fig. 1 [3]. This leads to unstable behavior that necessitates the use of a tailplane to stabilize the aircraft [2].

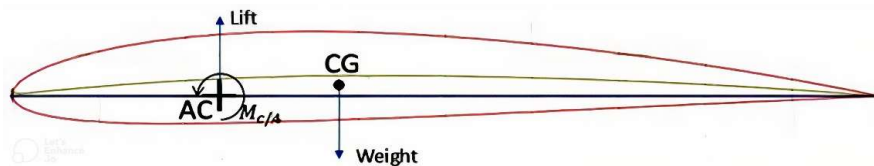


Fig. 1 Conventional airfoil in equilibrium position.

However, in flying wings, stability originates from the airfoil itself [1]. Reflexed airfoils are often used for this purpose. The reflex curvature changes the pressure distribution [4]. This alteration leads to negative lift near the trailing edge, which in turn changes the moment coefficient C_m to positive values. This change results in a positive pitching moment at AC. When a disturbance increases the AoA, the reflex airfoil generates a restoring moment that brings the AoA back toward equilibrium, see Fig. 2 [5].

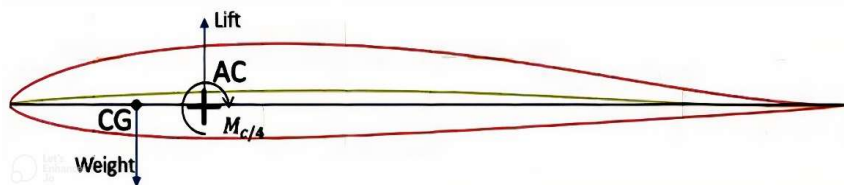


Fig. 2 Reflex airfoil in equilibrium.

2.2. Lateral stability

Lateral stability is the aircraft's capacity to return to its original roll angle following a disturbance. In flying wings, the aircraft relies instead on aerodynamic characteristics and proper mass distribution [8]. A lower center of mass improves lateral stability by enabling gravity to aid in the recovery process [1]. But aerodynamic effects, especially those arising from sideslip, play a crucial role. When an aircraft rolls, it usually sideslips, leading to asymmetric airflow across the wings and generating a corrective roll moment that assists in returning to level flight.

Rolling and yawing motions are closely interconnected. A roll disturbance often triggers yaw, and vice versa, making it challenging to analyze or maintain stability in one direction without affecting the other [6].

The dihedral effect can naturally correct roll. Wings featuring upward dihedral produce greater lift on the lower wing during sideslip, thereby creating a corrective roll moment. Also, flying wings achieve this effect through wing sweep, washout, or wing twist, which reroute airflow and enhance lateral damping [4].

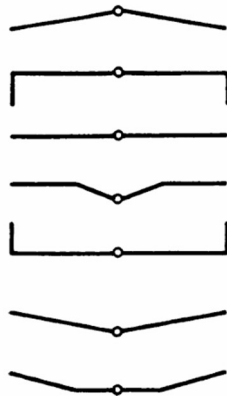


Fig. 3 Different flying wing configurations affect lateral stability [1].

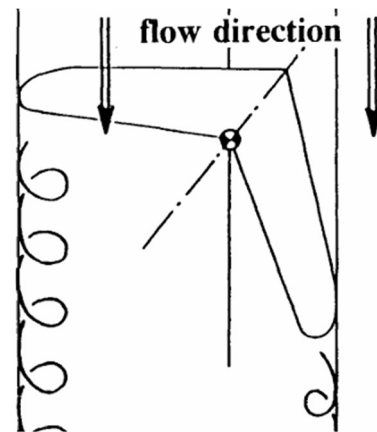


Fig. 4. Illustration of yawing by induced drag [1].

Directional stability, or yaw stability, refers to the aircraft's inclination to realign with its flight path after a yaw disturbance. Traditional airplanes use vertical stabilizers to generate a restoring yaw moment, while flying wings rely on design features such as wing sweep, wingtip fins, and differential drag between the wings **Chyba! Nenašiel sa žiaden zdroj odkazov.**[1],[8].

Swept wings enhance yaw-sideslip coupling by generating different lift and drag during yaw maneuvers [8]. The advancing wing, facing a higher effective airspeed, produces increased lift and drag, resulting in a stabilizing yaw moment [1]. Additionally, the induced drag, which rises with lift, contributes to stabilization by extending the moment duration arms, which can be seen in Fig. 4.

To address this challenge in tailless designs, engineers incorporate various features that can generate stabilizing yaw moments. One common approach is the addition of vertical elements such as fins, keels, or wingtip endplates [8]. These are often placed along the wing or integrated into the structure since flying wings typically lack a traditional fuselage.

Although “toe-in” endplates may appear beneficial at first glance, their stabilizing effect is usually only significant at large sideslip angles and has little influence during typical flight conditions [1]. Therefore, designers often rely on more integrated aerodynamic solutions.

3. FLYING WING MADE FROM SOLID FOAM AND ITS ANALYSIS

A UAV model was built to analyze the stability characteristics of a flying wing, using the MH-45 airfoil. The geometry and structure of the model were designed to meet both aerodynamic and stability needs. The model is shown in Fig. 5-6.

To evaluate the stability characteristics of the aircraft, both theoretical and experimental methods were employed. The theoretical modeling was conducted using XFLR5, a tool commonly used for low Reynolds number airfoil and wing analysis. Wind tunnel testing and free-flight trials were performed to validate the simulation results and observe real-world dynamic behavior.

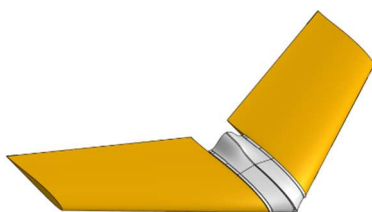


Fig. 5 Flying wing model in SolidWorks

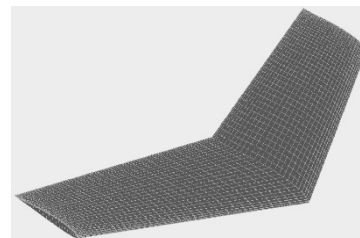


Fig. 6 Flying wing model in XFLR5

The aircraft had a wingspan of 0.750 m and a wing area of 0.190 m². The root chord measured 0.306 m, while the mean aerodynamic chord (MAC) was 0.257 m. The total mass of the aircraft was 0.635 kg. Based on these dimensions, the aspect ratio was calculated as 2.964 and the taper ratio as 0.654. The

wing loading was determined to be 3.347 kg/m^2 . The position of the neutral point was located at 0.191 m, and the center of gravity was positioned at 0.148 m from the leading edge.

3.1. Static longitudinal stability

To evaluate the longitudinal stability of the developed flying wing UAV, we used a combination of computer modeling and experimental testing. This process started with static stability analysis through XFLR5 simulations and wind tunnel tests, and was succeeded by dynamic stability assessments in both simulated and real flight environments.

Wind tunnel tests were conducted using a physical model of the flying wing, Fig. 7. The UAV was modified with additional structure to aid measurements. Support rods were installed at the wingtips to ensure the structure was properly aligned with the anticipated AC

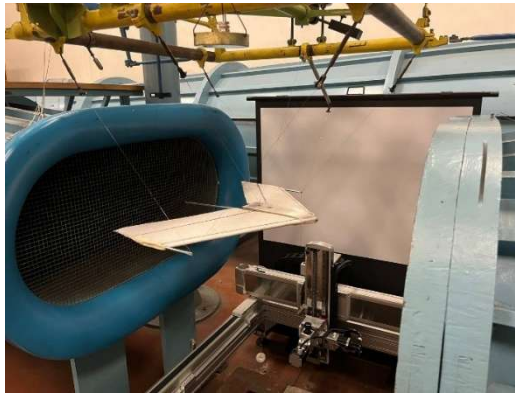


Fig. 7 UAV model in wind tunnel

Dynamic pressure was measured with the Scanivalve DSA 3217-PTP system, Fig. 8. Also, the balance system in the wind tunnel, Fig. 9, was used to measure lift (L), drag (D), and moment (M).



Fig. 8 Scanivalve DSA 3217-PTP



Fig. 9 Tunnel balances

Before testing, the DSA system was pre-heated for one hour to stabilize internal sensor properties and ensure accurate data. Atmospheric conditions were also recorded to allow correct non-dimensional coefficient calculation. These are presented below:

The flight tests were conducted at an altitude of 210 meters, with an ambient temperature of 292.95 K and atmospheric pressure of 745.6 mmHg. The relative humidity during the tests was 49.3%. Under these conditions, the air density was 0.888334 kg/m^3 . The dynamic viscosity of the air was $18.12 \times 10^{-6} \text{ Pa}\cdot\text{s}$.

The wind tunnel propulsion was turned on, stabilizing the flow at roughly 15 m/s. The aircraft underwent testing across AOA, of -5° , -2.5° , -1° , 0° , 1° , 2.5° , 5° , 7.5° , 10° , 12.5° , 15° , 20° , and 25° , with additional finer steps near the neutral and stall angles.

Throughout the testing, weight was added to the scales to balance the model and achieve equilibrium at each angle of attack. Aerodynamic forces and moments acting on the model during the tests. The results of the measurement can be seen in Table 1.

All measured forces and moments were recorded in grams; therefore, we first converted them to Newtons by multiplying to 0.009809, after which we applied the following formula for calculation.

$$C_L = \frac{L \cdot g}{q \cdot S} = \frac{-106.5 \cdot 0.009809}{140.2 \cdot 0.19} = -0.039 \quad (3.1.1)$$

To calculate the moment coefficient, we must apply a different formula. First, we convert g to kilograms by multiplying to 0.001, then convert this value to Newton-meters and multiply by the distance of the moment arm 0.2 m, over which the balancing system supports the additional weight. Since our system model is inverted, all subsequent values will have the opposite sign.

$$C_m = \frac{M \cdot 0.001 \cdot g \cdot l}{q \cdot S \cdot c} = \frac{48 \cdot 0.001 \cdot 9.809 \cdot 0.2}{140.2 \cdot 0.19 \cdot 0.2567} = -0.0138 \quad (3.1.2)$$

To calculate the drag moment, it is necessary to convert the measurements to Newtons by multiplying by 0.009809. For a more accurate value, we must also subtract the drag of the string that holds the entire model. Overall, we have 12 strings with a string diameter of 0.3 mm, a drag coefficient C_{DW} of 1.32, and an area formed by a perpendicular length of the string of 0.25 m.

$$C_D = \frac{D \cdot g}{q \cdot S} - C_{DW} \cdot \frac{S_w \cdot n}{S_M} = \frac{79.4 \cdot 0.009809}{140.2 \cdot 0.19} - 1.32 \cdot \frac{0.003 \cdot 0.25 \cdot 12}{0.19} = 0.023 \quad (3.1.3)$$

Table. 1 Result of wind tunnel testing

α [degrees]	Δp [Pa]	q [Pa]	L [N]	C_L	M [Nm]	C_m	D [N]	C_D
-5	139.1	140.213	-1.045	-0.039	-0.094	-0.014	0.779	0.023
-2.5	135.3	136.382	1.349	0.052	-0.028	-0.004	0.745	0.022
-1	137.0	138.096	2.526	0.096	0.005	0.001	0.827	0.025
0	139.3	140.414	3.541	0.133	0.010	0.003	0.922	0.028
1	138.6	139.709	4.512	0.170	0.053	0.008	1.010	0.032
2.5	138.5	139.608	5.640	0.213	0.060	0.009	1.116	0.036
5	130.9	131.947	6.719	0.268	0.099	0.015	1.291	0.045
7.5	133.0	134.064	7.033	0.276	0.156	0.024	1.793	0.064
10	132.6	133.661	8.892	0.350	0.173	0.027	2.209	0.081
12.5	129.5	130.536	10.295	0.415	0.166	0.026	2.786	0.106
15	127.9	128.923	11.663	0.476	0.171	0.027	3.655	0.143
20	119.2	120.154	12.869	0.564	0.074	0.012	6.080	0.260
25	119.4	120.355	13.311	0.582	-0.307	-0.052	7.477	0.321

Dimensionless data from Table. 1, is presented in Figs. 10-12.

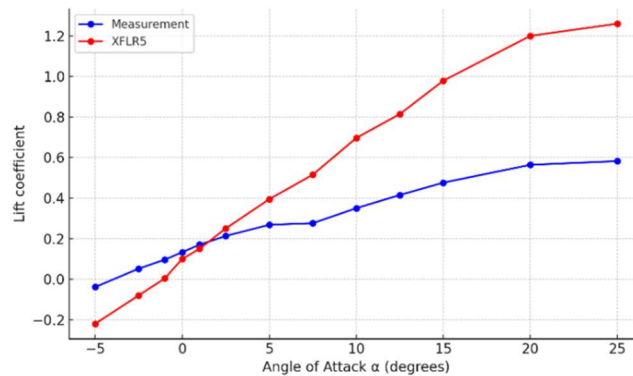


Fig. 10 Graph C_L vs α from measuring in the wind tunnel

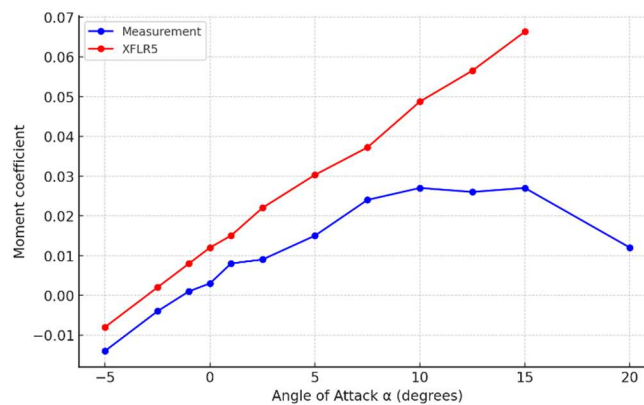


Fig. 11 Graph C_m vs α from measuring in the wind tunnel test

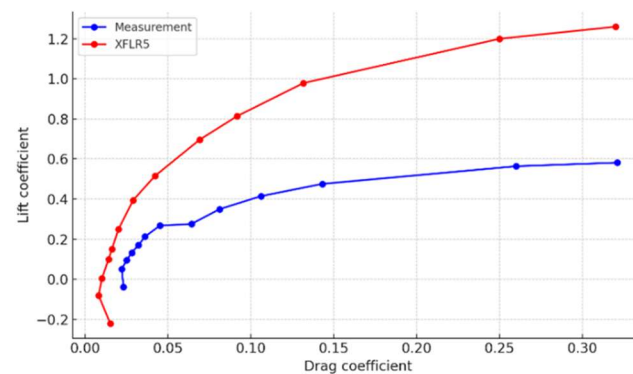


Fig. 12 Graph C_L vs C_d from measuring in the wind tunnel test

The aerodynamic stability of the flying wing configuration depends on the pitching moment coefficient C_m in relation to the AoA, α , in Fig. 11. Experimental wind tunnel results show that C_m rises with α across a wide range, demonstrating a positive slope. This behavior confirms that the configuration exhibits static longitudinal instability.

The positive pitching moment slope and negative C_m at C_L equate to 0, indicating that the existing flying wing flap configuration is unstable, and the reference pitch axis is behind the AC.

The physical model was made from EEP, a soft and flexible material. As the AoA increased, the model's trailing edge visibly bent due to airflow, likely influencing its aerodynamic performance. The wind tunnel measurements had known uncertainties: ± 2 g for lift, ± 0.2 g for moment, and ± 5 g for drag. These uncertainties were particularly important for moment and drag, which tend to be naturally small. A significant challenge during the experiment was maintaining true system equilibrium. Structural

imperfections in the weight-measuring apparatus meant that even slight disturbances often disrupted the force equilibrium. As a result, each measurement point needed multiple adjustments and precise weight corrections to ensure stable and reliable results.

3.2. Dynamic stability

XFLR5 model was used to simulate longitudinal and lateral motions Fig.13-14.

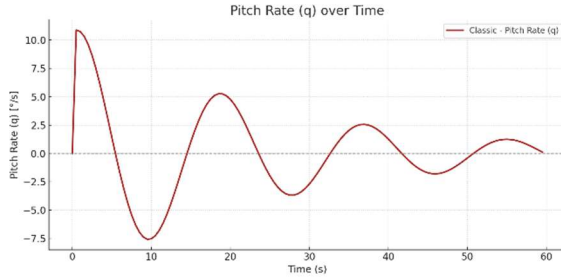


Fig. 13 The XFLR5 simulation of longitudinal motion

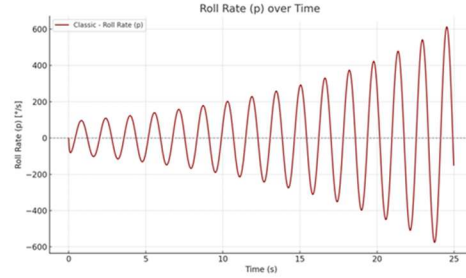


Fig. 14 The XFLR5 simulation of lateral motion

From simulated data, we can readily see that our UAV is longitudinally stable but laterally unstable. For better analysis, we describe these graphs with stability equations. Longitudinal motion can be described by the equation:

$$\theta(t) = Ae^{-\zeta\omega_n t} \cos(\omega_d t + \phi) \quad (3.2.1)$$

The average time period of longitudinal oscillations is:

$$T = \frac{T_1+T_2+T_3+T_4+T_5}{5} = \frac{10.5+11+.5+10.5+10.5}{5} = 10,6 \text{ s} \quad (3.2.2)$$

The damping frequency, damping rate, damping ratio calculation, and natural frequency:

$$\omega_d = \frac{2\pi}{T} = \omega_d = \frac{2\pi}{10.6} = 0.593 \frac{\text{rad}}{\text{s}} \quad (3.2.3)$$

$$d = \frac{\ln\left(\frac{A_i}{A_{i+1}}\right)}{t_{i+1}-t_i} \quad (3.2.4)$$

$$d = \frac{d_1+d_2+d_3+d_4+d_5}{5} = \frac{0.043+.041+0.042+0.042+0.045}{5} = 0.042 \frac{1}{\text{s}} \quad (3.2.5)$$

$$\omega_n = \sqrt{\omega_d^2 + d^2} = \sqrt{0.593^2 + 0.042^2} = 0.595 \frac{\text{rad}}{\text{s}} \quad (3.2.6)$$

$$\zeta = \frac{d}{\omega_n} = \frac{0.042}{0.595} = 0.071 \quad (3.2.7)$$

The damping ratio ($\zeta = 0.071$), according to the theory, it is underdamped $0 < \zeta < 1$, oscillations gradually decay toward a stable state. The three remaining elements: the initial derivative $\dot{x}(0)$, phase angle, and amplitude.

$$\dot{x}(0) = \frac{x(t_1)-x(0)}{t_1-0} = \frac{5.052-7.931}{11-0.5} = -0.274 \frac{\text{deg}}{\text{s}} \quad (3.2.8)$$

$$A = \sqrt{x(0)^2 + \left(\frac{\dot{x}(0)}{\omega_d}\right)^2} = \sqrt{7.931 + \left(\frac{-0.274}{0.593}\right)^2} = 7.94 \text{ deg} \quad (3.2.9)$$

$$\phi = \arctan\left(-\frac{\dot{x}(0)}{\omega_d \cdot x(0)}\right) = \arctan\left(-\frac{-0.274}{0.593 \cdot 7.931}\right) = 0.058 \text{ rad} \quad (3.2.10)$$

Final longitudinal dynamic model is:

$$\theta(t) = 7.94 \cdot e^{-0.071 \cdot 0.595 \cdot t} \cos(0.593 \cdot t + 0.058) \quad (3.2.11)$$

Analogous steps were used to get the lateral dynamic model:

$$\beta(t) = 82.75 \cdot e^{-(-0.01) \cdot 7.85 \cdot t} \cos(7.854 \cdot t + 0.39) \quad (3.2.12)$$

The negative damping ratio $\zeta = -0.01$ means that this UAV is laterally unstable.

After conducting wind dynamic simulations that confirmed the static longitudinal stability of the flying wing model, the subsequent step involved testing its dynamic stability during actual flights. This flight test was designed to assess the UAV dynamic longitudinal stability by monitoring its responses to

slight pitch disturbances and comparing the actual outcomes with those predicted by XFLR5 simulations. The model utilized for collecting flight data is shown in Fig. 15.



Fig. 15 Model for flight tests

The flying wing featured an onboard accelerometer and gyroscope to capture angular accelerations and pitch rate performance during flight. The wind speed was measured at 7.2 m/s, with an ambient temperature of 273.15 K. The relative humidity was 71%, and the atmospheric pressure was recorded at 763.29 mmHg.

A brief entry on the control surface generated a managed pitch disturbance. The accelerometer documented the flying wing's oscillatory reaction. The data was post-processed to extract the damping ratio, natural frequency, and oscillation amplitude, utilizing the UAV Log Viewer website to log readings. For more accurate measurements, several recordings were taken during UAV launches. The result from measuring can be seen in Fig. 16-17.

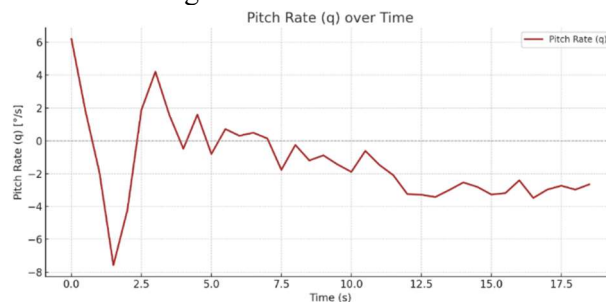


Fig. 16 Longitudinal dynamics from flight measurements

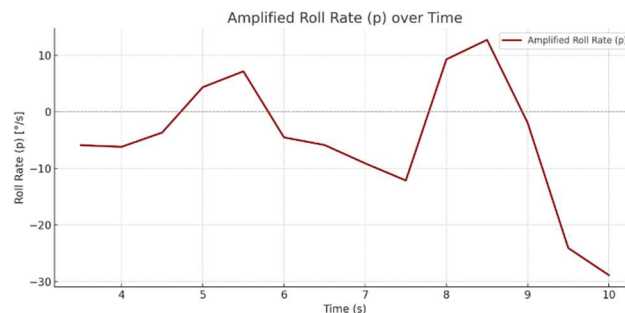


Fig. 17 Lateral dynamics from flight measurements

A natural frequency and damping ratio from flight tests confirm those predicted by XFLR5 dynamic stability module.

4. CONCLUSION

This study provided an evaluation of the static and dynamic stability of a tailless aircraft through computer simulations, wind tunnel testing, and flight tests. Simulations from the XFLR5 provided the aft limit form CG position. Despite the structural flexibility of the EPP model used, the results confirmed the XFLR5 prediction.

Dynamic simulations showed that the UAV is longitudinally stable but laterally unstable. The longitudinal damping ratio and natural frequency obtained from the simulations were in close agreement with the actual flight test data, confirming the underdamped, self-correcting pitch oscillations. However, the lateral instability observed in both the simulations and the flight data indicates a critical limitation of the model design in its current form, likely due to the lack of vertical stabilizing surfaces or sufficient dihedral effect.

Overall, the results of the study highlight that tailless aircraft can achieve stable flight through careful aerodynamic shaping, especially through the use of reflex airfoils and appropriate center of gravity placement. However, additional improvements, such as improved roll and yaw stability solutions, are essential for fully stable flight. The methodology presented in this study provides a reproducible framework for evaluating the stability of unconventional aircraft, supporting the further development of flying wing UAVs and similar tailless aircraft.

5. LITERATURE LIST

- [1] NICKEL, K. - Wohlfahrt, M. 1994. *Tailless aircraft in theory & practice*. Washington: American Institute of Aeronautics and Astronautics, Inc., 1994. 498 p. ISBN 15-6347-094-2
- [2] DORE, F. 1947. *The Design of Tailless Airplanes*. California: Institute of Technology, 1947. 53 p. [DOI 10.7907/ORZ6-EV10](https://doi.org/10.7907/ORZ6-EV10)
- [3] CHALIA, S. 2017. *Design Characteristics of an Airfoil for Flying/ Tailless Wings: A Study*. Noida: Department of Aerospace Engineering Amity University Haryana, 2017. 3 p. [ISSN 2321-061-3](https://doi.org/10.21203/rs.3.rs-1000000/v1)
- [4] SCHÜRMEYER, C. 1985. *Development of Airfoil Sections for the Swept-Back Tailless Sailplane SB-13*. Braunschweig: Akademische Fliegergruppe, 2018. 6 p. <https://journals.sfu.ca/ts/index.php/op/article/view/1984>
- [5] MARSKE, J. 1970. *Experiment in flying wing sailplanes*. Michigan: The Soaring Society of America, 1970. 54 p.
- [6] ROSKAM, J. 2001. *Airplane Flight Dynamics and Automatic Flight Controls: Part I*. Kansas: Dwsign, Analysis and Research Corporation (DARcorporation), 2001. 608 p. ISBN 1-884885-179
- [7] ESTEBAN, S. 2001. *Static and Dynamic Analysis of an Unconventional Plane: Flying Wing*. Montreal: American Institute of Aeronautics and Astronautics, 2001. 16 p. [AIAA-2001-4010](https://doi.org/10.2514/6.2001-1010)
- [8] ROBERT, T.J. 1970. *Note on the Stability of Tailless Aircraft*. Washington: Langley Memorial Aeronautical Laboratory, 1941. 26 p. [NACA Technical Note No. 837](https://ntrs.nasa.gov/archive/0000019/corpusid/1970001-1)

received 5, 2025, accepted 6, 2025



Article is licensed under a Creative Commons Attribution 4.0 International License